ER-positive breast cancer cells are poised for RET-mediated endocrine resistance

Sachi Horibata[1,2], Edward J. Rice[1], Chinatsu Mukai[1], Brooke A. Marks[1], Kelly Sams[1], Hui Zheng[1], Lynne J. Anguish[1], Scott A. Coonrod[1,3]*, Charles G. Danko[1,3]*

1 Baker Institute for Animal Health, College of Veterinary Medicine, Cornell University, Ithaca, NY, United States of America, **2** Department of Molecular Medicine, College of Veterinary Medicine, Cornell University, Ithaca, NY, United States of America, **3** Department of Biomedical Sciences, College of Veterinary Medicine, Cornell University, Ithaca, NY, United States of America

* dankoc@gmail.com (CGD); sac269@cornell.edu (SAC)

Abstract

The RET tyrosine kinase signaling pathway is involved in the development of endocrine resistant ER+ breast cancer. However, we know little about how ER+ cells activate RET signaling and initiate an endocrine resistant phenotype. Here we show that both ER+ endocrine resistant and sensitive breast cancers have a functional RET tyrosine kinase signaling pathway, but that endocrine sensitive breast cancer cells lack RET ligands that are necessary to drive endocrine resistance. Transcription of one RET ligand, GDNF, is necessary and sufficient to confer resistance in the ER+ MCF-7 cell line. Endogenous GDNF produced by endocrine resistant cells is translated, secreted into the media, and activates RET signaling in nearby cells. In patients, RET ligand expression predicts responsiveness to endocrine therapies and correlates with survival. Collectively, our findings show that ER+ tumor cells are "poised" for RET mediated endocrine resistance, expressing all components of the RET signaling pathway, but endocrine sensitive cells lack high expression of RET ligands that are necessary to initiate the resistance phenotype.

Introduction

Estrogen receptor alpha (ERα) is the major driver of ~75% of all breast cancers. Current therapies for patients ith ER+ breast cancer are largely aimed at blocking the ERα signaling pathway. For example, tamoxifen blocks ERα function by competitively inhibiting E2/ERα interactions [1] and fulvestrant promotes ubiquitin-mediated degradation of ERα [2]. Endocrine therapies are estimated to have reduced breast cancer mortality by 25–30% [3]. However, despite the widespread success of endocrine therapies, approximately 40–50% of breast cancer patients will either present with endocrine-resistant breast cancer at the time of diagnosis or progress into endocrine-resistant disease during the course of treatment [4]. Thus, there remains an urgent need to further elucidate the mechanism of endocrine resistance.

Numerous studies have now identified growth factor-stimulated signaling "escape" pathways that may provide mechanisms for cell growth and survival that are independent of E2. Foremost among these, the RET tyrosine kinase signaling pathway has been associated with

endocrine resistance in both cell culture models as well as in primary tissues [5–8]. These studies have led to effective new biomarkers based on the downstream targets of RET signaling [6]. However, resistance by the RET signaling pathway has proven complex, relying in some cases on a functional ERα to drive resistance in aromatase inhibitor models [6]. Furthermore, genetic alterations in RET or its co-receptor, GFRA1, do not appear to be common in clinical cases, suggesting that additional factors are involved. A better understanding of the transcriptional targets of RET-mediated signaling pathways as well as understanding how these pathways crosstalk with ERα signaling will likely aid in the development of new predictive biomarkers and new targets for therapeutic intervention.

Here, we used Precision Run-On and Sequencing (PRO-seq) to comprehensively map RNA polymerase in tamoxifen-sensitive (TamS) and resistant (TamR) MCF-7 cells [9]. This approach is highly sensitive to immediate and transient transcriptional responses to stimuli, allowing the discovery of target genes within minutes of activation [10–14]. Moreover, active transcriptional regulatory elements (TREs) can be detected by this method, including both promoters and distal enhancers, as these elements display distinctive patterns of transcription that can aid in their identification [15–20]. Among the 527 genes and 1,452 TREs that differ in TamS and TamR MCF-7 cells, we identified glial cell line-derived neurotrophic factor (GDNF), a ligand of RET tyrosine kinase receptor, to be upregulated in TamR MCF-7 cells. Remarkably, we found that all of the proteins necessary to drive endocrine resistance through RET receptor signaling are expressed in TamS MCF-7 cells, with the exception of a single limiting protein, GDNF or any of the other RET ligands (GDNF, NRTN, ARTN, or PSPN). To test this model, we manipulated GDNF expression in MCF-7 cells and found that high GDNF expression is both necessary and sufficient for tamoxifen resistance in our MCF-7 cell model. Several lines of evidence suggest that RET ligands are the limiting reagent in clinical samples as well, including ample expression of RET and its co-receptors, but limiting expression of GDNF and the other RET ligands in primary tumors. Additionally, RET ligand expression is predictive of responsiveness to endocrine therapies in breast cancer patients. Taken together, our studies support a model in which tamoxifen sensitive and resistant cells are 'poised' for RET-mediated endocrine resistance by expressing RET and its co-receptor, but are limited by the abundance of RET ligands to drive a resistant phenotype.

Results

Transcriptional differences between endocrine sensitive and resistant MCF-7 cells

Although MCF-7 cells are ER+ and usually require E2 for growth and proliferation, a subset of the heterogeneous MCF-7 cell population continues to grow in the presence of anti-estrogens such as tamoxifen [9,21]. We hypothesized that the resistant cells display a unique transcriptional program which can be used to identify factors that play a causative role in tamoxifen resistance. We used PRO-seq to map the location and orientation of RNA polymerase in two tamoxifen sensitive (TamS) and two *de novo* resistant (TamR) MCF-7 cell lines that were clonally derived from parental MCF-7 cells [9]. Consistent with the Gonzalez-Malerva study, we found that the TamS lines (TamS; B7^{TamS} and C11^{TamS}) were sensitive to as little as 1 nM of tamoxifen, while the TamR lines (TamR; G11^{TamR} and H9^{TamR}) were not affected at concentrations as high as 100 nM (Fig 1A). PRO-seq libraries were prepared from all four cell lines (Fig 1B), as previously described [22,23], and sequenced to a combined depth of 87 million uniquely mapped reads (S1 Table). We quantified the similarity of transcription in the MCF-7 cell subclones by comparing the Pol II abundance in annotated gene bodies. Unbiased hierarchical clustering grouped B7^{TamS} and C11^{TamS} TamS lines into a cluster and left G11^{TamR} and
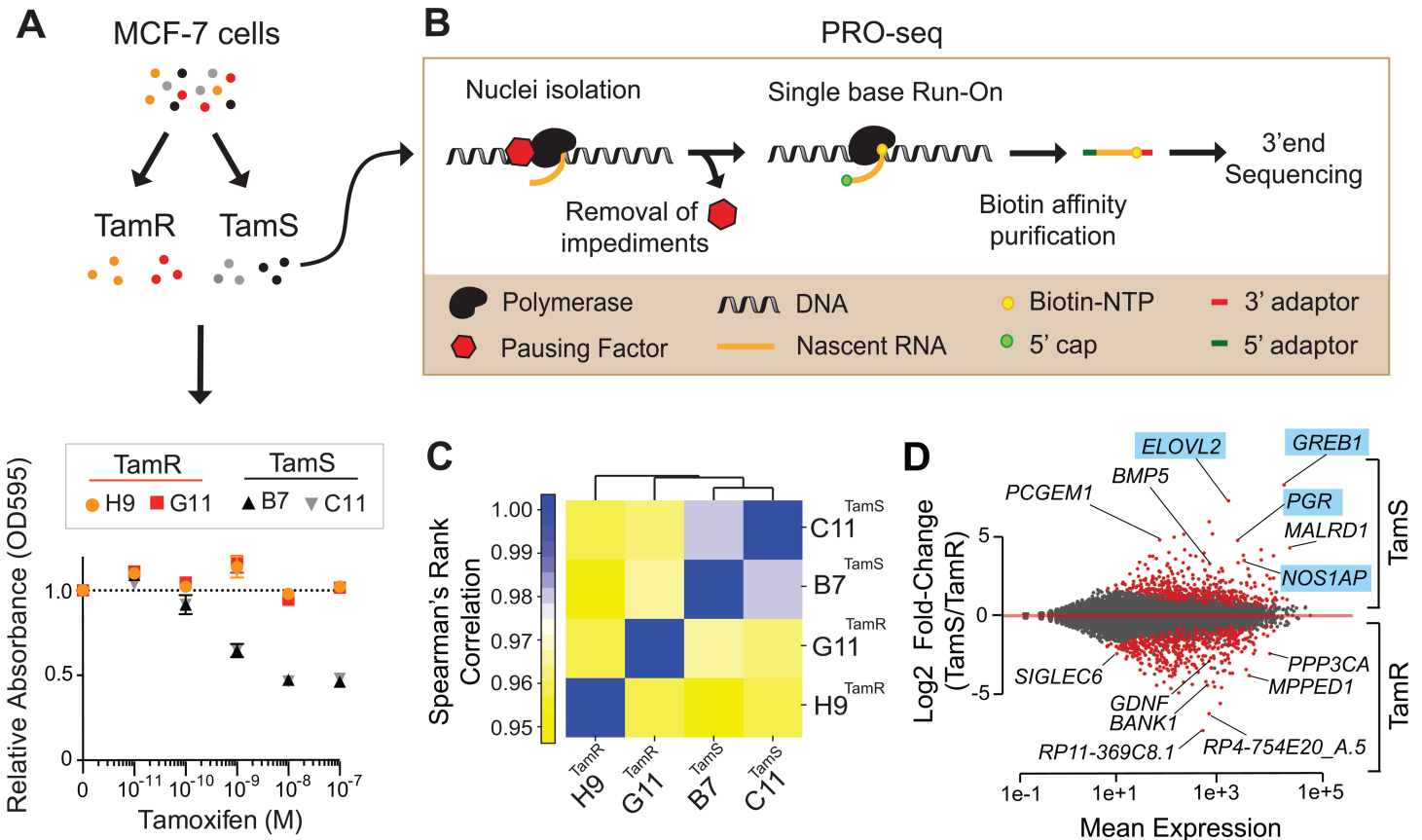
Fig 1. PRO-seq provides a genome-wide location of active RNA polymerase. (a) Cell viability of tamoxifen sensitive (TamS; B7^{TamS} and C11^{TamS}) and resistant (TamR; G11^{TamR} and H9^{TamR}) MCF-7 cells upon treatment with 0 (vehicle; EtOH), 10^{-11}, 10^{-10}, 10^{-9}, 10^{-8}, or 10^{-7} M of tamoxifen for 4 days. Data are represented as mean ± SEM (n = 3). (**b**) Experimental setup for PRO-seq. PRO-seq libraries were prepared from all four cell lines grown in the absence of tamoxifen for 3 days. (**c**) Spearman's rank correlation of RNA polymerase abundance in the gene bodies (+1000 bp to the annotation end) of TamS and TamR cell lines. (**d**) MA plot showing significantly changed genes (red) that are higher in TamS (top) or TamR (bottom) MCF-7 lines. Genes highlighted in the plots which are ERα targets are highlighted in blue.

H9^{TamR} TamR lines as more distantly related outgroups (Fig 1C). Although TamR cells clustered independently, all four MCF-7 clones are nevertheless remarkably highly correlated (Spearman's Rho > 0.95), suggesting that relatively few transcriptional changes are necessary to produce the tamoxifen resistance phenotype.

We identified 527 genes that are differentially transcribed between TamS and TamR MCF-7 cells (1% FDR, DESeq2 [24]), 341 of which were transcribed more highly in TamS and 186 more highly in TamR cell lines (Fig 1D). Several of the differentially transcribed genes, including, for example, *PGR*, *GREB1*, and *GDNF*, were identified in other models of endocrine resistance [6,7,25–28], supporting our hypothesis that transcriptional changes in the MCF-7 model are informative about endocrine resistance.

ER target genes are uniquely expressed in tamoxifen-sensitive MCF-7 cells

To confirm that transcriptional changes detected using PRO-seq lead to differences in mRNA abundance, we validated transcriptional changes in *PGR* (Fig 2A) and *GREB1* (Fig 2B) between the B7^{TamS} and G11^{TamR} MCF-7 cells using qPCR (Fig 2C and 2D). Many of the differentially transcribed genes are targets of ERα signaling, including *PGR*, *GREB1*, *NOS1AP*, and *ELOVL2*, (Fig 1D) suggesting that changes between TamR and TamS MCF-7 cells can be explained in
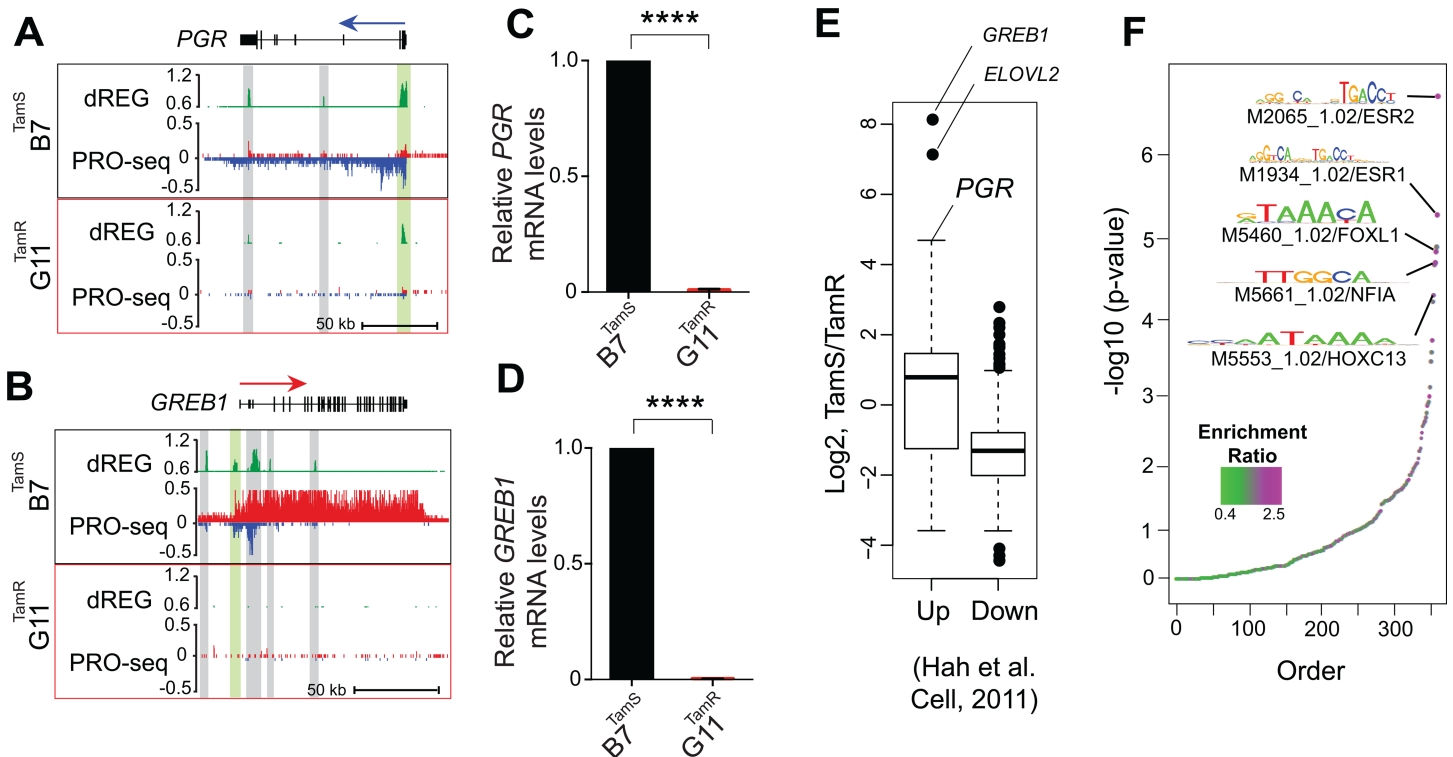
Fig 2. ER target genes are uniquely expressed in TamS cells. (**a-b**) Transcription near the *PGR* (**a**) and *GREB1* (**b**) loci in B7^{TamS} and G11^{TamR} cells. PRO-seq densities on the sense and anti-sense strand are shown in red and blue, respectively. dREG scores are shown in green. Enhancers and promoters are shown in grey and light green shading, respectively. Arrows indicate the direction of gene annotations. (**c-d**) *PGR* (**c**) and *GREB1* (**d**) mRNA expression levels in B7^{TamS} and G11^{TamR} cells. Data are represented as mean ± SEM (n = 3 for *PGR*; n = 4 for *GREB1*). **** $p < 0.0001$. G11^{TamR} is normalized to B7^{TamS}. (**e**) Boxplots represent fold-change between TamS and TamR of genes that are either up- or down-regulated following 40 minutes of estrogen (E2) in Hah et. al. (2011). Spearman's Rho = 0.185, $p < 2.2e-16$. (**f**) Motifs enriched in TREs that have different amounts of RNA polymerase between TamS and TamR cells compared with TREs that have consistent levels.

part by differences in the genomic actions of ERα. To test for an enrichment of ERα target genes, we used an independent GRO-seq dataset [10] to investigate whether immediate transcriptional changes following E2 treatment are correlated with genome-wide changes in TamS and TamR MCF-7 cells. We found that genes up-regulated by 40 minutes of E2 treatment tend to be transcribed more highly in TamS MCF-7 cells, and genes down-regulated by E2 are more highly transcribed in TamR cell lines (Fig 2E). Thus, our data demonstrate global changes in the genomic actions of ERα in tamoxifen resistance in this MCF-7 model system.

Distal enhancer activities correlate with tamoxifen resistance

To elucidate the mechanisms responsible for changes in gene transcription during the development of tamoxifen resistance, we sought to discover the location of promoters and active distal enhancers, collectively called transcriptional regulatory elements (TREs). Nascent transcription is a sensitive way to identify groups of active enhancers [16–19], and results in enhancer predictions that are highly similar to the canonical active enhancer mark, acetylation of histone 3 at lysine 27 (H3K27ac) [17,18,29]. We used our dREG software package [18] followed by a peak refinement that identifies the regions between divergent paused RNA polymerase [30] to identify 39,753 TREs that were active in either the TamS or TamR MCF-7 lines. TREs discovered using dREG were highly enriched for other active enhancer and promoter marks in MCF-7 cells, especially H3K27ac (S1A Fig), as expected based on prior studies [16–18,29]. As an example, we selected a transcribed enhancer downstream of the *CCND1* gene for

experimental validation using luciferase reporter gene assays, and confirmed luciferase activity in both B7^{TamS} and G11^{TamR} MCF-7 cells (S1B and S1C Fig).

We used the abundance of RNA polymerase recruited to each TRE as a proxy for its transcriptional activity in each MCF-7 subclone to identify differences in 1,452 TREs (812 increased and 640 decreased) (1% FDR, DESeq2) between TamS and TamR MCF-7 cells. Differentially transcribed TREs were frequently located near differentially expressed genes and undergo correlated transcriptional changes between the four MCF-7 subclones. *GREB1* and *PGR*, for example, are each located near several TREs, including both promoters (green) and enhancers (gray), which undergo changes between TamR and TamS MCF-7 cells that are similar in direction and magnitude to those of the primary transcription unit which encodes the mRNA (Fig 2A and 2B). These results are consistent with a broad correlation between changes at distal TREs and protein coding promoters [10,16].

We hypothesized that differential transcription at TREs reflects differences in the binding of specific transcription factors that coordinate changes between TamS and TamR lines. We identified 12 clusters of motifs enriched in TREs that are differentially active in the TamS and TamR lines (Bonferroni corrected p< 0.05; RTFBSDB [31]). The top scoring motif in this analysis corresponds to an estrogen response element (ERE), the canonical DNA binding sequence that recruits ERα to estrogen responsive enhancers (Fig 2F). At least two of the top scoring motifs, those that were putatively bound by NFIA and HOX-family transcription factors (HOXC13 shown), bind a transcription factor that was itself differentially expressed in TamS and TamR MCF-7 cells (Fig 2F), consistent with our expectation that transcriptional changes of a transcription factor elicit secondary effects on the activity of TREs, and downstream effects on gene transcription.

ERα signaling remains functional in endocrine-resistant lines

GREB1 and *PGR* play a critical role in ERα genomic activity in breast cancer cells [27,32]. Our observation that transcription of these ERα co-factors was lost in the resistant lines (Fig 2A, 2B, 2C and 2D) suggests that ERα signaling may be defective in the TamR cell lines. Consistent with this expectation, several analyses (i.e., the enrichment of ERα target genes and EREs, Fig 1G and 1H) implicate global changes in the genomic actions of ERα during the development of tamoxifen resistance. However, these analyses are correlative and do not directly test the immediate responses to E2 in TamR and TamS lines.

To directly test the hypothesis that the genomic actions of ERα are substantially altered in the TamR lines, we treated B7^{TamS} and G11^{TamR} MCF-7 cells for 40 minutes with either E2 or tamoxifen, and monitored transcriptional changes using PRO-seq. RNA polymerase abundance increased sharply at ERα ChIP-seq peaks [33] in B7^{TamS} MCF-7 cells (Fig 3A top) in response to E2, but not in response to tamoxifen, in agreement with our prior work [11,16]. Although we observed a muted effect of E2 on enhancers in G11^{TamR} compared with B7^{TamS}, increases in Pol II loading were observed in response to E2, but not tamoxifen (Fig 3A bottom). These results demonstrate that E2 signaling pathway remains functional and able to affect gene transcription in a stimulus-dependent manner in TamR cells. We attribute the muted response in G11^{TamR} to a 2.44-fold reduction in the abundance of ERα mRNA in G11^{TamR} MCF-7 cells compared to the B7^{TamS} MCF-7 cells (Fig 3B). This muted effect explains the enrichment in E2 target genes, as well as the ERE motif enrichment, between TamS and TamR lines shown in Figs 1 and 2. Nevertheless, the genomic actions of E2-liganded ERα remain functional in TamR MCF-7 cells.

Given that E2 signaling remains functional, but muted in the TamR line, we next tested whether ERα was required for the growth of our tamoxifen-resistant cells. We found that the viability of both G11^{TamR} and H9^{TamR} MCF-7 cells was unaffected by treatment with the ER degrader, fulvestrant (Fig 3C). Therefore, endocrine resistance in G11^{TamR} and H9^{TamR} MCF-7
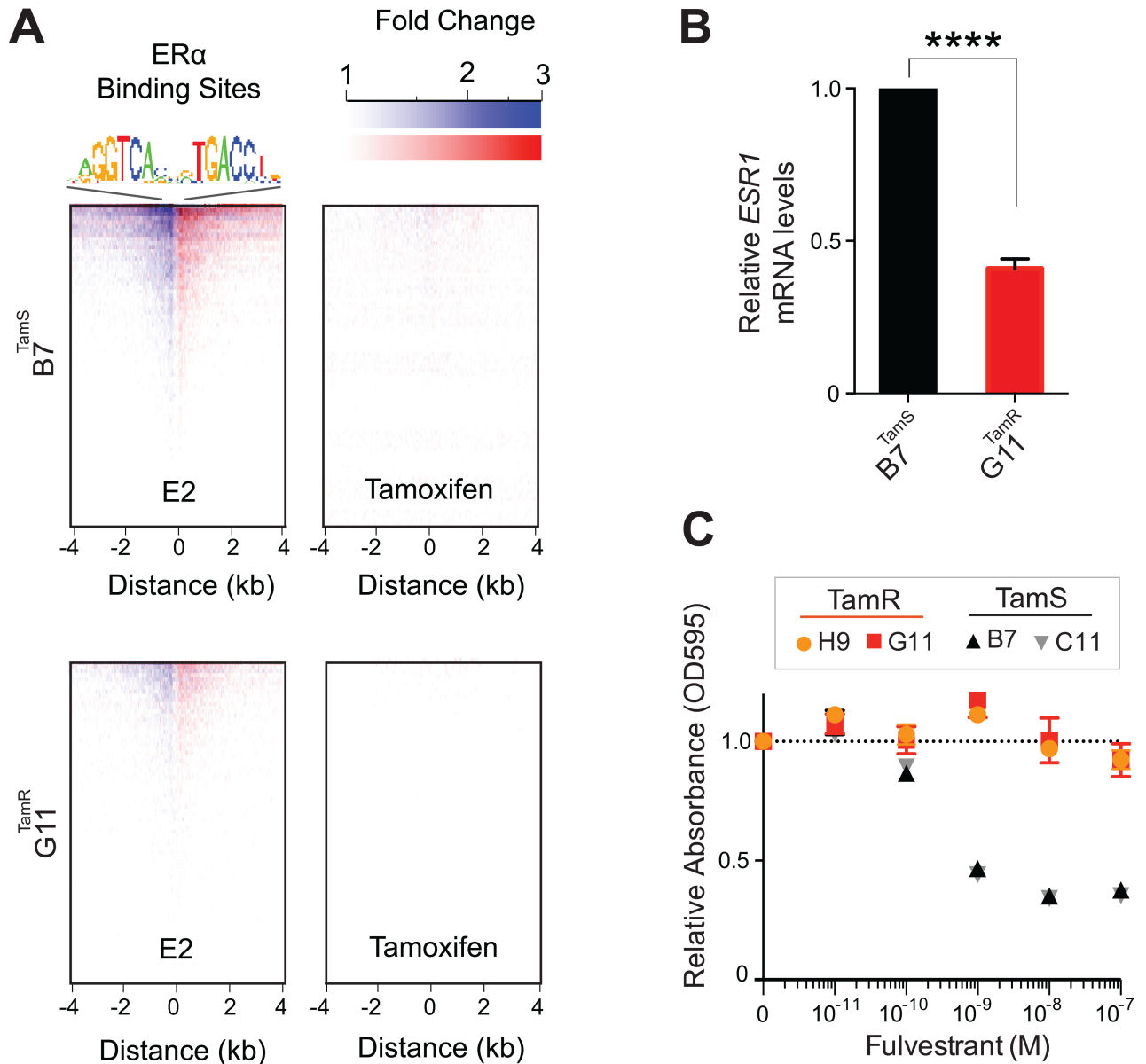
Fig 3. Tamoxifen resistant lines have functional ERα signaling. (**a**) Heatmap of changes in RNA polymerase abundance following 40 minutes of E2 or tamoxifen treatment near ERα bindings sites in B7^{TamS} and G11^{TamR} cells. (**b**) *ESR1* mRNA expression levels in B7^{TamS} and G11^{TamR} cells. Data are represented as mean ± SEM (n = 3). **** p < 0.0001. (**c**) Cell viability of TamS and TamR cells upon treatment with 0 (vehicle; DMSO), 10^{-11}, 10^{-10}, 10^{-9}, 10^{-8}, or 10^{-7} M fulvestrant (ER degrader) for 4 days. Data are represented as mean ± SEM (n = 3).

https://doi.org/10.1371/journal.pone.0194023.g003

cells appears to occur independently of ERα signaling, suggesting that these TamR lines are likely using an alternative pathway for cell survival and proliferation when grown in the presence of tamoxifen.

GDNF is necessary and sufficient to confer endocrine resistance in MCF-7 cells

We next investigated pathways by which TamR lines may promote cell survival in the presence of endocrine therapies. Tyrosine kinase growth factor signaling pathways have been implicated

in preclinical models of endocrine resistance [5,7,34]. RET is a cell surface receptor that elicits cell survival signals when bound by one of four RET ligands, GDNF, NRTN, ARTN, and PSPN [35]. One of these ligands, glial cell line-derived neurotrophic factor (GDNF), was among the most highly up-regulated genes in both G11[TamR] and H9[TamR] MCF-7 lines (Fig 4A). We confirmed the transcriptional differences in *GDNF* between B7[TamS] and G11[TamR] MCF-7 cells using qPCR and found that GDNF mRNA levels were increased by ~25 fold in the resistant line (Fig 4B). We asked whether GDNF mRNA is translated into protein and secreted into the
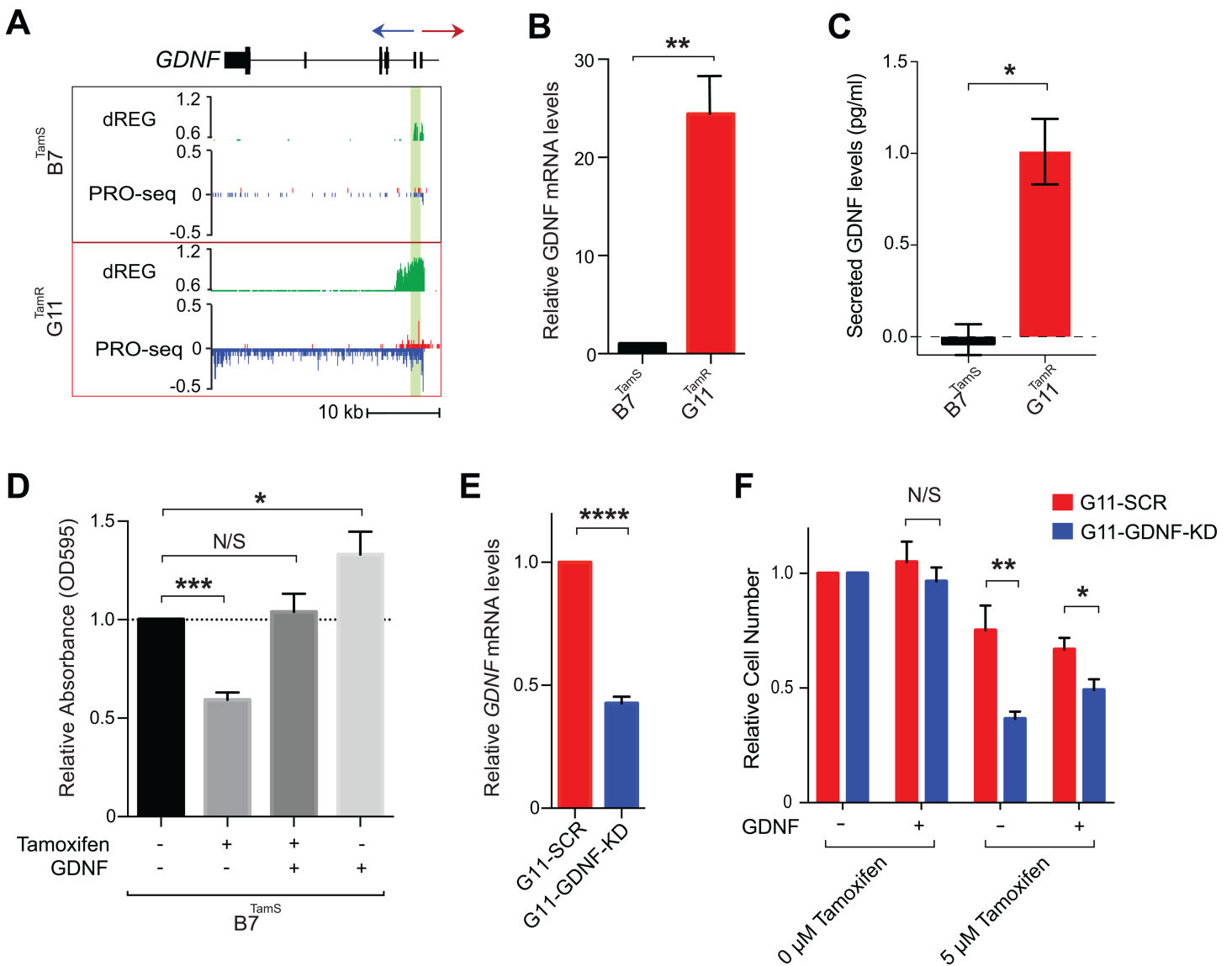

Fig 4. *GDNF* is responsible for tamoxifen resistance in MCF-7 cells. (**a**) Transcription near the *GDNF* locus in B7[TamS] and G11[TamR] cells. PRO-seq densities on sense strand and anti-sense strand are shown in red and blue, respectively. dREG scores are shown in green. The region near the GDNF promoter is shown in light green shading. Arrow indicates the direction of gene annotations. (**b**) *GDNF* mRNA expression levels in B7[TamS] and G11[TamR] cells. Data are represented as mean ± SEM (n = 3). ** $p < 0.005$. (**c**) Secreted GDNF levels in B7[TamS] and G11[TamR] cells. Data are represented as mean ± SEM (n = 2). * $p < 0.05$. (**d**) Cell viability of B7[TamS] cells in the presence or absence of 10 ng/ml GDNF and/or 100 mM tamoxifen for 4 days. Data are represented as mean ± SEM (n = 3). * $p < 0.05$, *** $p < 0.0005$. (**e**) *GDNF* mRNA expression levels in G11[TamR] scrambled (SCR) and G11[TamR] GDNF knockdown (GDNF-KD) cells. Data are represented as mean ± SEM (n = 3). **** $p < 0.0001$. (**f**) Relative cell number of G11[TamR] scrambled (SCR) and G11[TamR] GDNF knockdown (GDNF-KD) cells after 4 days without or with 5 μM tamoxifen and/or 5 ng/ml GDNF treatment. Data are represented as mean ± SEM (n = 9). * $p < 0.05$, ** $p < 0.005$.

media, and thereby could be acting to activate RET signaling in nearby cells. Using an ELISA we found GDNF accumulates in media collected from G11^{TamR} MCF-7 cells, but was undetectable in B7^{TamS} MCF-7 cells (Fig 4C). Thus GDNF transcription, mRNA abundance, and GDNF protein secretion correlate with endocrine resistance in MCF-7 cells, suggesting that GDNF may contribute to the endocrine resistance phenotype.

We tested whether GDNF is casually involved in endocrine resistance by manipulating GNDF levels in our MCF-7 model. We first examined the effects of 10 ng/mL of recombinant GDNF protein on the growth of B7^{TamS} cells in the presence of antiestrogens. Remarkably, GDNF completely rescued B7^{TamS} MCF-7 cells when challenged with both tamoxifen (Fig 4D) and fulvestrant (ER degrader) (S2A Fig). This shows that ER does not need to be present nor functional for GDNF-induced endocrine resistance. Moreover, GDNF treatment without tamoxifen increased the proliferation rate of B7^{TamS} MCF-7 cells by ~20% (Fig 4D), suggesting that the growth pathways activated by GDNF can work independently of ERα. Next we tested whether GDNF was necessary to confer endocrine resistance in our model system by using short hairpin RNAs (shRNA) to knockdown GDNF in G11^{TamR} MCF-7 cells. Results show that GDNF depletion (GDNF-KD) reduced *GDNF* mRNA levels by 57.38% (Fig 4E) and that these cells were significantly more sensitive to tamoxifen treatment than G11 cells transfected with a scrambled control (Fig 4F). Moreover, endocrine resistance could be restored to GDNF-KD G11 cells by the addition of 5 ng/ mL recombinant GDNF protein (Fig 4F), demonstrating that growth inhibition does not reflect an off-target effect of the *GDNF* shRNA. Taken together, these data demonstrate that *GDNF* plays a central and causal role in establishing endocrine resistance in G11^{TamR} MCF-7 cells.

Endocrine-sensitive ER+ breast cancer cells express RET transmembrane receptors

Having shown that *GDNF* expression promotes endocrine resistance in our MCF-7 cell model, we asked whether *GDNF* promotes resistance in patients as well. Increases in the expression of RET tyrosine kinase or its co-receptor GFRα1 are thought to be involved in endocrine resistance [5–7]. However, RET is itself transcriptionally activated by ERα and is highly abundant in endocrine sensitive ER+ breast cancer cell models [10]. Analysis of mRNA-seq data from 1,177 primary breast cancers in the cancer genome atlas (TCGA) revealed that the RET mRNA expression level was highest in ER+ breast cancer and correlates positively with the expression level of *ESR1* (ERα) (Spearman's $\rho = 0.51$, $p < 2.2e-16$; Fig 5A), suggesting that it is a direct transcriptional target of ERα *in vivo* as well. *GFRA1* mRNA encodes the GDNF co-receptor, GFRα1, and, together with RET, activates RET-ligand signaling. Further analysis of the mRNA-seq data set found that *GFRA1* is also strongly correlated with *ESR1* mRNA in breast cancers (Spearman's $\rho = 0.52$, $p < 2.2e-16$; S3A Fig), suggesting that it is also a direct target of E2 signaling. In our MCF-7 endocrine resistance model, *GFRA1* transcription is 5-fold higher in TamS MCF-7 cells compared to TamR lines and *RET* transcription is not significantly different (Fig 5B and 5C), demonstrating that neither factor is overexpressed in TamR MCF-7 cells. Since both RET and GFRA1 are naturally high in ER+ breast cancer cells, and since high expression of these factors appears to be established in part by ERα, there must be other causes of endocrine resistance, both in cell models and *in vivo*.

ER+ breast cancer cells and primary breast cancers that are sensitive to endocrine therapy lack GDNF to initiate resistance

Our finding that recombinant GDNF was sufficient for endocrine resistance in B7^{TamS} MCF-7 cells demonstrates that GDNF is a key limiting factor, the absence of which prevents TamS
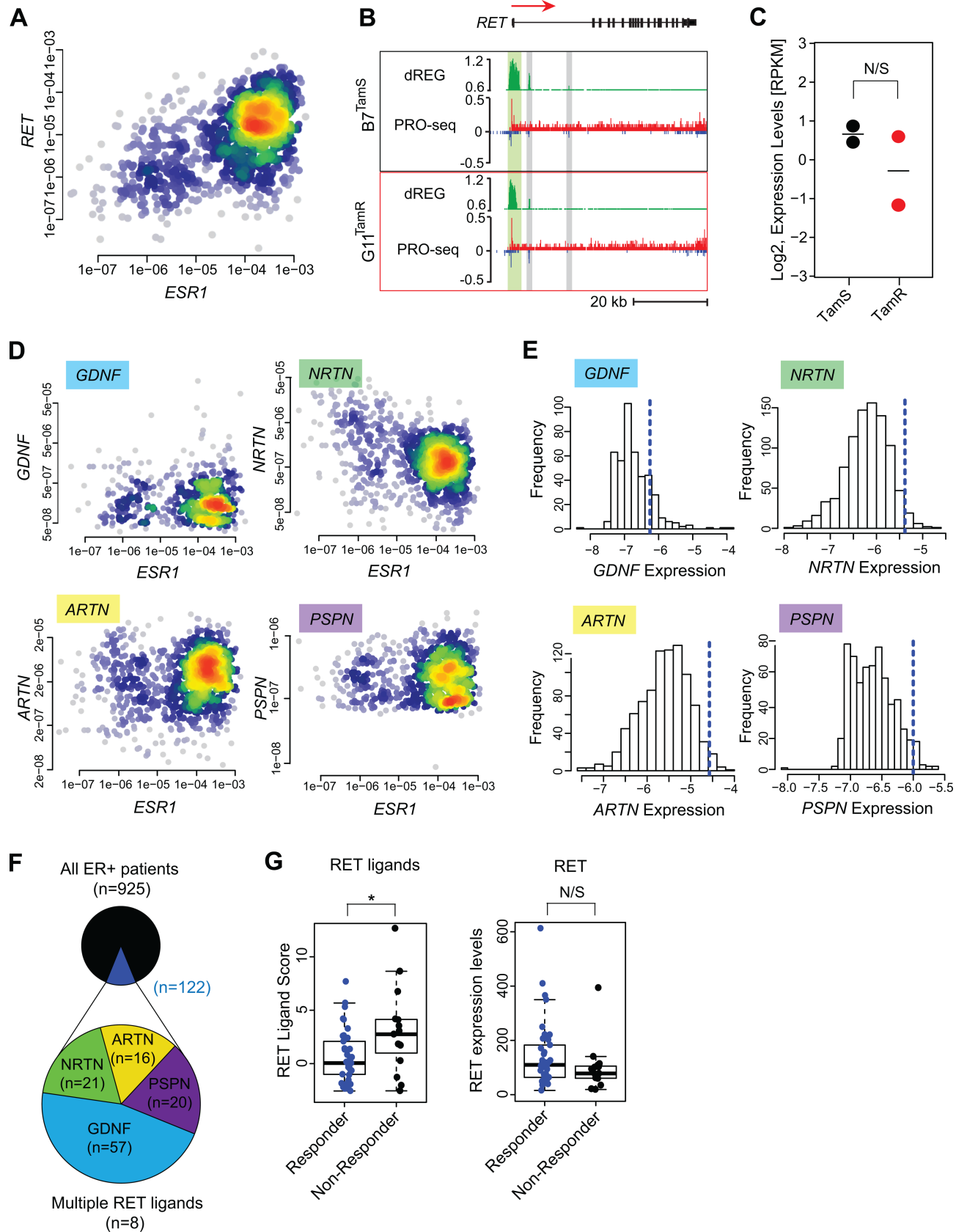
Fig 5. Expression of RET ligands contributes to endocrine resistance. (**a**) Density scatterplot showing *RET* and *ESR1* expression in mRNA-seq data from 1,177 primary breast cancer models in the cancer genome atlas (TCGA). Spearman's ρ = 0.51, *p* = 1.2e-60. (**b**) Transcription near the *RET* locus in B7^{TamS} and G11^{TamR} cells. PRO-seq densities on sense strand and anti-sense strand are shown in red and blue, respectively. dREG scores are shown in green. Enhancers and promoters are shown in grey and light green shading, respectively. Arrow indicates the directional movement of transcribed genes. (**c**) Dot plot shows *RET* transcription levels in TamS and TamR MCF-7 cells. (**d**) Density scatterplots show the expression of RET ligands (*GDNF*, *NRTN*, *ARTN*, and *PSPN*) versus *ESR1* based on mRNA-seq data from 1,177 primary breast cancers. (**e**) RET ligand expression distribution in ER + breast cancers. The dotted blue line represents 2.5 times the range between the 25th and 50th percentile. (**f**) Fraction of ER+ breast cancers (n = 925) with at least one RET ligand exceeding the threshold shown in panel E (shown in dark blue, n = 122). Among the 4 RET ligands, GDNF was the most highly expressed (n = 60). (**g**) Boxplots show RET ligands score and RET expression levels in patients that respond or do not respond to aromatase inhibitor letrozole. * *p* = 0.016.

cells from developing a resistant phenotype. To extend this hypothesis to primary breast cancers, we sought to determine whether GDNF expression is normally low, such that it might limit RET pathway activation in most ER+ breast cancers. Indeed, GDNF expression was detectible in only 565 of 1,177 primary breast cancers (48%) analyzed by TCGA (S3B Fig). In principal, RET signaling may be activated by any of the four RET ligands (GDNF, NRTN, ARTN, and PSPN). However, only low levels of NRTN, ARTN, or their co-receptors were detected in primary breast tumors (Figs 5D, 5E and S3B). Thus, we conclude that RET ligand expression is low compared with that of cell surface receptors, especially RET and GFRα1, which are activated in part by ERα. This contrast between RET receptors and ligands supports a model in which the RET signaling pathway is 'poised' for endocrine resistance by expression of the receptors and that limiting levels of *GDNF* expression, or possibly other RET ligands, would ensure endocrine sensitivity in most tumors.

Next, we investigated whether high RET ligand expression in a subset of ER+ tumors may explain some cases of endocrine resistance. A careful examination of the GDNF expression distribution in TCGA breast cancers revealed a long tail, indicating high GDNF expression in a subset of cases in the TCGA dataset (Fig 5E). Our hypothesis that GDNF expression limits RET-dependent endocrine resistance implies that these GDNF-high samples should be prone to endocrine resistance. We devised a simple non-parametric computational approach, which we call the 'outlier score', to quantify the degree to which GDNF is highly expressed based on the symmetry of the empirical probability density function (see Methods; Fig 5E, blue line). Based on this score, we conservatively estimate that, of 925 ER+ breast cancer patients in the TCGA dataset, 122 have high expression of at least one of the RET ligands (13%), 57 of which had high levels of GDNF (Fig 5F).

If RET ligands are the limiting factor for endocrine resistance, as we propose here, cases included in this long distribution tail are those that are more likely to be resistant to endocrine therapies. To test this hypothesis, we analyzed expression microarray data collected prospectively by biopsies of patients that either respond, or do not respond, to the aromatase inhibitor letrozole [36]. A score comprised of the sum of the outlier scores from all four RET ligands is significantly higher in patients that do not respond to letrozole treatment (p = 0.016, one-sided Wilcoxon rank sum test; Fig 5G). By contrast, there is no significant difference in RET expression in patients who respond or who do not respond to letrozole. These results suggest that RET ligand expression, but not RET itself, explain the differences in response to letrozole in this cohort of patients.

Discussion

In this study, we have used genomic tools to dissect how the GDNF-RET signaling pathway becomes activated in breast cancer cells to promote resistance to endocrine therapies. Systematic experimental manipulation of GDNF expression in TamS and TamR cell lines build on work described in previous studies [5–8] by providing the strongest support yet for this pathway

playing a causal role in endocrine resistance in MCF-7 cells. To extrapolate these findings to breast cancer patients we have conducted a detailed statistical analysis of data collected from primary breast cancers. Furthermore, analysis of clinical data supports a model in which *RET* and *GFRA1* are actively transcribed in both endocrine sensitive MCF-7 cells and primary tumors, awaiting RET ligands to initiate resistance to endocrine therapies. This is, to our knowledge, the first study to suggest that expression of RET ligands themselves (including GDNF, ARTN, NRTN, and PSPN) are responsible for RET-mediated endocrine resistance. Overall, our study provides insights into how the RET signaling pathway become activated in ER+ breast cancers.

We suggest that RET-mediated endocrine resistance occurs when ER+ breast cancer cells express the RET ligand GDNF. Work on the RET signaling pathway in endocrine resistance has largely focused on amplifications or increases in the expression of RET or its co-receptor GFRα1 in resistance to aromatase inhibitors [6,7]. However, RET expression is not significantly different in a cohort of patients resistant to the aromatase inhibitor letrozole (Fig 5G), suggesting that other mechanisms may occur more commonly in patients than differences in the expression of RET itself. Indeed, we find that expression of RET and GFRα1 are both highest in ER+ breast cancers, likely because of direct transcriptional activation of both genes by E2/ ERα (Figs 5A and S3A). Thus, we propose that ER+ breast cancer cells are intrinsically 'poised' for RET-mediated endocrine resistance by the activation of RET cell-surface receptors, but lack expression of the ligand GDNF.

Based on our findings, we hypothesize that increased expression of any one of the four RET ligands, GDNF, ARTN, NRTN, or PSPN confers endocrine resistance on cells expressing the RET receptor. In support of this model, we demonstrate that the scoring system we used, based on RET ligand overexpression in tumors, clearly separates breast cancer patients that respond to letrozole from those who do not (Fig 5G). Several findings also strongly support the involvement of GDNF in endocrine resistance in our MCF-7 model, most notably the observations that GDNF rescues B7^{TamS} lines and that GDNF knockdown in G11 cells restores sensitivity to tamoxifen (Fig 4F). These observations are also supported by existing studies showing that another RET ligand, ARTN, contributes to tamoxifen resistance in MCF-7 cells [37], extending and supporting the findings reported here. However, there is one RET ligand that is notably an outlier. PSPN does not appear to have any predictive value in patients, and thus may not play the same role in resistance as the other three RET ligands. This may reflect the extremely low expression of its co-receptor, *GFRA4*, in primary breast cancers (S3B Fig), preventing PSPN from having much effect on breast cancer cells. Taken together, these findings suggest that RET ligand expression, especially GDNF, ARTN, and NRTN, explain endocrine resistance in many cases.

We also found evidence that ERα may itself play an important role in establishing expression of the RET receptor and its GFRA1 co-receptor in breast cancer cells. RET is a well-characterized direct ERα target in cell lines [10,38]. By a comparison of RNA-seq data in primary breast cancers (Figs 5A and S3), we show that both RET and GFRA1 correlate with expression of ESR1, suggesting that they may be targets of ERα signaling in primary tumors. We also show that GDNF promotes resistance in an ERα independent manner, as demonstrated by insensitivity of TamR cells to ER degradation by fulvestrant. Taken together, our findings demonstrate that ERα may contribute to expression of RET receptors in ER+ cells, but that it's actions are dispensable to maintain resistance after the expression GDNF or other RET receptors.

Another important question is whether our findings based on the MCF-7 model are a general mechanism of endocrine resistance. To determine whether GDNF is an important contributor to primary breast tumors, we have conducted a detailed statistical analysis of publicly available data. Our analyses found a correlation between RET ligand expression and resistance

to aromatase inhibitors (Fig 5G). Moreover, we also show that mRNA abundance of both RET and GFRA1 correlate with ESR1 across primary breast cancers (Figs 5A and S3A), suggesting that RET and GFRA1 are direct targets of ERα signaling in primary patients as well. Taken together with our cell-based model, these findings suggest that RET ligands are an important factor that initiates endocrine resistance across biological systems.

A major question that remains unclear and of primary importance following our study is how RET ligand expression becomes activated in primary tumors. The abundance of GDNF mRNA appears to be extremely low in primary breast tumors analyzed by TCGA (Figs 5D, 5E and S3B), which were in most cases collected before therapeutic intervention [39,40]. Notably, GDNF is not natively expressed in ER+ TamS MCF-7 cells but rather becomes activated following extended endocrine treatments. This may suggest that GDNF expression is initiated in tumors by another stimulus-dependent pathway or introduced by another cell type in the tumor microenvironment. We show in a companion paper that GDNF-RET stimulation indirectly activates transcription of the endogenous GDNF gene [ref: Horibata et. al. (2018) PLoS One]. Therefore one possibility is that GDNF becomes expressed after tumor cells are "primed" with GDNF by another cell in the microenvironment. Another possibility is that GDNF expression in tumors may be initiated by pro-inflammatory cytokines, such as tumor necrosis factor alpha (TNFα), to be transcribed in breast cancer cells [28]. This finding may link poor survival outcomes in pro-inflammatory tumors [41,42] with GDNF-RET-mediated resistance to endocrine therapy.

Finally, we also do not know whether RET ligands are responsible for all types of endocrine resistance. We found a clear distinction in one cohort of patients treated with letrozole (Fig 5G). Intriguingly, the RET ligand expression score is elevated in this subset of patients prior to treatment, suggesting that RET ligands promote an intrinsic (rather than acquired) mode of endocrine resistance. Whether RET ligands also play a role in resistance following recurrence in cases where tumors previously responded remains unknown.

Taken together, results reported in this study implicate RET ligands, including GDNF, as the primary determinant of endocrine resistance in both MCF-7 cells and patient samples (Fig 6). Clinical studies targeting larger cohorts of patients beginning endocrine therapies will be required to fully validate our proposed mechanism of endocrine resistance.

Methods

Cell lines and cell culture

Tamoxifen-sensitive (TamS; B7^{TamS} and C11^{TamS}) and resistant (TamR; G11^{TamR} and H9^{TamR}) MCF-7 cells[9] were a gift from Dr. Joshua LaBaer. TamS cells were grown in Dulbecco's Modified Eagle Medium (DMEM) supplemented with 5% fetal bovine serum (FBS) and 1% Penicillin Streptomycin, and TamR cells were grown in the same media supplemented with 1 μM tamoxifen. Tamoxifen used throughout in this paper is (Z)-4-Hydroxytamoxifen (4-OHT; Sigma-Aldrich; Cat# H7904).

Cell viability assay

Briefly, 5 x 10^3 TamS and TamR cells were grown in 24-well TC-treated plates in their specific culture media. After allowing the cells to adhere to the plate for 24 hours, they were rinsed with PBS three times to remove any residual tamoxifen. The cells were treated with either increasing doses of tamoxifen (0 (vehicle control; EtOH), 10^{-11}, 10^{-10}, 10^{-9}, 10^{-8}, or 10^{-7} M).

For setting up the rescue experiment with GDNF (PeproTech; Cat# 450–10), 5 x 10^3 B7^{TamS} cells were grown in 24-well TC-treated plates in their specific culture media. After allowing the cells to adhere to the plate for 24 hours, they were treated with either EtOH (vehicle), 10^{-7} M
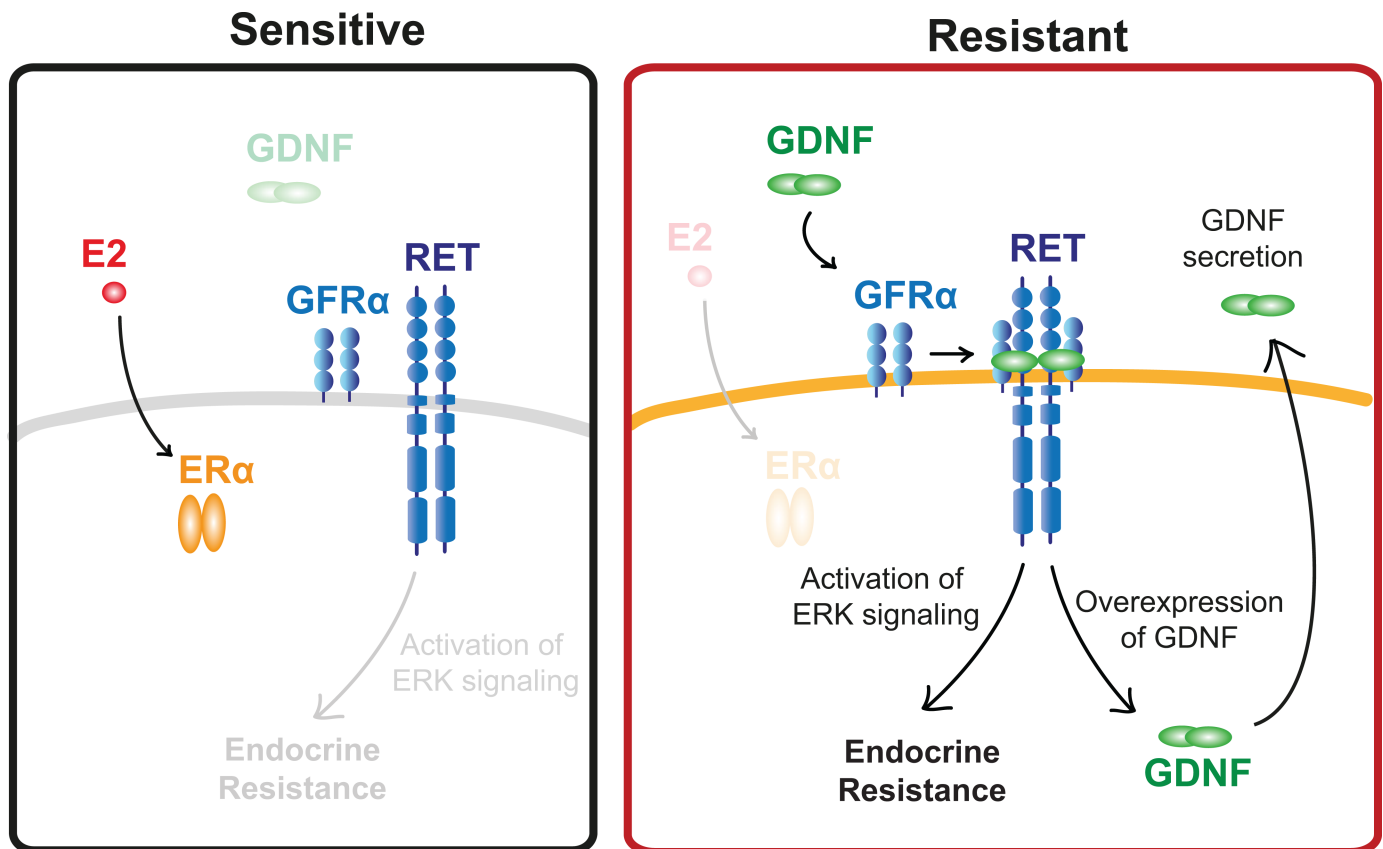
Fig 6. Schematic diagram of RET activation in endocrine sensitive and resistant tumors. Both endocrine sensitive and resistant breast cancer cells express all components of the RET signaling pathway, but endocrine sensitive breast cancer cells lack GDNF to initiate the resistance pathway. By contrast, endocrine resistant cells secret GNDF, which acts in an autocrine or paracrine fashion to promote endocrine resistance in nearby cells.

tamoxifen, 10^{-7} M tamoxifen and 10 ng/mL GDNF, or 10 ng/mL GDNF treatment. The same set up was performed for 10^{-7} M treatment of fulvestrant and using DMSO (vehicle) as a control.

After four days of endocrine treatment, cells were fixed with 4% paraformaldehyde and stained with 0.5% crystal violet solution made in 25% methanol. After washing away non-specific crystal violet stain with PBS, we took pictures of each plate and the crystal violet stain from the fixed cells was removed using 10% acetic acid. The absorbance was measured using the Tecan plate reader at OD_{595nm}. Samples were normalized to the untreated control. Three biological replicates were performed and data are represented as mean ± SEM.

ELISA

TamS (B7^{TamS}) and TamR (G11^{TamR}) lines were plated on 6 well plate at 70% confluency. Cells were washed with PBS and fresh media (DMEM supplemented with 5% FBS) was added the next day. 96 hours later, media was collected and were concentrated with Amicon Ultra-4 centrifugal filter units (Millipore; MWCO 3000). GDNF levels were measured using ELISA kit (Abcam; Cat# ab100525) according to the manufacturers' protocol.

Cell culture set up and nuclei isolation

TamS and TamR lines were grown in 150mm TC-treated culture dishes in their respective normal culture media. Cells were rinsed with PBS at least three times 24 hours after plating.

Both the TamS and TamR cells were grown in Dulbecco's Modified Eagle Medium supplemented with 5% fetal bovine serum and 1% Penicillin Streptomycin for an additional three days until ~80% confluency in the absence of tamoxifen, in order to measure the difference between TamS and TamR cells pre-treatment.

Nuclei were isolated as described previously [43]. Briefly, cells were rinsed three times with ice-cold PBS and lysed using lysis buffer (10 mM Tris-HCl pH 7.4, 2 mM MgCl$_2$, 3 mM CaCl$_2$, 0.5% NP-40, 10% Glycerol, 1 mM DTT, 1X PIC (Roche; Cat# 11836153001), and 1 μl/10 mL SUPERase-In (ThermoFisher; Cat# AM2694) dissolved in DEPC water). Cells were homogenized by gently pipetting at least 30 times and the nuclei were harvested by centrifugation at 1000 g for five minutes at 4°C. The isolated nuclei were washed twice with lysis buffer and were resuspended in 100 μL freezing buffer (50 mM Tris HCl pH 8.3, 5 mM MgCl$_2$, 40% Glycerol, 0.1 mM EDTA pH 8.0, and 4 U/mL SUPERase-In). The isolated nuclei were used for nuclear run-on and precision nuclear run-on sequencing (PRO-seq) library preparation.

Nuclear run-on and PRO-seq library preparation

Nuclear run-on experiments were performed according to the methods described previously [22,23]. 1x10^7 nuclei in 100 μL freezing buffer were mixed with 100 μL of 2x nuclear run-on buffer (10 mM Tris-HCl pH 8.0, 5 mM MgCl2, 1 mM DTT, 300 mM KCl, 50 μM biotin-11-ATP (Perkin Elmer; Cat# NEL544001EA), 50 μM biotin-11-GTP (Perkin Elmer; Cat# NEL545001EA), 50 μM biotin-11-CTP (Perkin Elmer Cat# NEL542001EA), 50 μM biotin-11-UTP (Perkin Elmer; Cat# NEL543001EA), 0.4 units/μL SUPERase In RNase Inhibitor (Life Technologies; Cat# AM2694), 1% Sarkosyl (Fisher Scientific; Cat# AC612075000). The mixture was incubated at 37°C for five minutes. The biotin run-on reaction was stopped using Trizol (Life Technolgies; Cat# 15596–026), Trizol LS (Life Technologies; Cat# 10296–010) and pelleted. The use of GlycoBlue (Ambion; Cat# AM9515) is recommended for higher pellet yield. RNA pellets were re-dissolved in DEPC water and denatured in 65°C for 40 seconds and hydrolyzed in 0.2 N NaOH on ice for 10 minutes to have a hydrolyzed RNA length with that range ideally of 40 to 100 nts. Bead binding (NEB; Cat# S1421S) was performed to pull down nascent RNAs followed by 3' RNA adaptor ligation (NEB; Cat# M0204L). Another bead binding was performed followed by 5' de-capping using RppH (NEB; Cat# M0356S). 5' phosphorylation was performed followed by 5' adaptor ligation. The last bead binding was performed before generation of cDNA by reverse transcription. PRO-seq libraries were prepared according to manufacturers' protocol (Illumina) and were sequenced using the Illumina NextSeq500 sequencing.

Mapping of PRO-seq sequencing reads

PRO-seq reads failing Illumina quality filters were removed. Adapters were trimmed from the 3' end of remaining reads using cutadapt with a 10% error rate [44]. Reads were mapped with BWA[45] to the human reference genome (hg19) and a single copy of the Pol I ribosomal RNA transcription unit (GenBank ID# U13369.1). The location of the RNA polymerase active site was represented by a single base that denotes the 3' end of the nascent RNA, which corresponded to the position on the 5' end of each sequenced read. Mapped reads were normalized to reads per kilobase per million mapped (RPKM) and converted to bigWig format using Bed-Tools[46] and the bedGraphToBigWig program in the Kent Source software package[47]. Downstream data analysis was preformed using the bigWig software package, available from: https://github.com/andrelmartins/bigWig. All data processing and visualization was done in the R statistical environment[48].

Identification of active enhancers and promoters using dREG-HD

We identified TREs using dREG [18]. Data collected from all four cell lines (TamR and TamS MCF-7 cells) was combined to increase statistical power for the discovery of a superset of TREs active during any of the conditions examined.

The precise coordinates of TREs were refined using a strategy that we termed dREG-HD (available at https://github.com/Danko-Lab/dREG.HD; manuscript in preparation). Briefly, dREG-HD uses an epsilon-support vector regression (SVR) with a Gaussian kernel to map the distribution of PRO-seq reads to DNase-I signal intensities. Training was conducted on randomly chosen positions within dREG peaks in K562 cells (GEO ID# GSM1480327) extended by 200bp on either side. We selected the optimal set of features based on maximizing the Pearson correlation coefficient between the imputed and experimental DNase-I signal intensity over an independent validation set. Before DNase-I imputation, PRO-seq data was preprocessed by normalizing read counts to the sequencing depth and scaled such that the maximum value was within the 90th percentile of the training examples. To identify peaks, we smoothed the imputed DNase-I signal using a cubic spline and identified local maxima. We tuned the performance of the peak by empirically optimizing two free parameters that control the (1) smoothness of spline curve fitting, and (2) a threshold level on the intensity of the imputed DNase-I signal. Parameters were optimized to achieve <10% false discovery rates on a K562 training dataset by a grid optimization over free parameters. We tested the optimized dREG-HD model (including both DNase-I imputation and peak calling) a GRO-seq dataset completely held out from model training and parameter optimization in on GM12878 lymphoblastoid cell lines (GSM1480326). Testing verified that dREG-HD identified transcribed DNase-I hypersensitive sites with 82% sensitivity at a 10% false discovery rate.

Additional genomic data in MCF-7 cells generated by the ENCODE project was downloaded from Gene Expression Omnibus. TREs discovered using dREG-HD were compared with ChIP-seq for H3K27ac and H3K4me3 (accession numbers: GSM945854 and GSM945269) and DNase-1 hypersensitivity (GSM945854).

Differential expression analysis (DESeq2)

We compared treatment conditions or cell lines using gene annotations (GENCODE v19). We counted reads in the interval between 1,000 bp downstream of the annotated transcription start site to the end of the gene for comparisons between TamS and TamR cell clones. To quantify transcription at enhancers, we counted reads on both strands in the window covered by each dREG-HD site. Differential expression analysis was conducted using deSeq2 [24] and differentially expressed genes were defined as those with a false discovery rate (FDR) less than 0.01.

Motif enrichment analysis

Motif enrichment analyses were completed using the default set of 1,964 human motifs in RTFBSDB[31] clustered into 622 maximally distinct DNA binding specificities (see ref Wang et. al. (2016)). We selected the motif to represent each cluster with canonical transcription factors that were most highly transcribed in MCF-7 cells. We fixed the motif cutoff log odds ratio of 7.5 (log e) in a sequence compared with a third-order Markov model as background. We identified motifs enriched in dREG-HD TREs that change transcription abundance between two conditions using Fisher's exact test with a Bonferroni correction for multiple hypothesis testing. TREs were compared to a background set of >1,500 GC-content matched TREs that do not change transcription levels (<0.25 absolute difference in magnitude (log-2 scale) and $p > 0.2$) using the enrichmentTest function in RTFBSDB[31].

TCGA data analysis

Processed and normalized breast cancer RNA-seq data was downloaded from the International Cancer Genome Consortium (ICGC) data portal website (https://dcc.icgc.org). Data profiling each gene was extracted using shell scripts. Processing and visualization was done in R.

Letrozole microarray reanalysis

We reanalyzed Affymetrix U133A microarray data profiling mammary tumor biopsies before and after treatment with letrozole[36]. Miller et. al. (2012) collected data from mammary tumor biopsies prior to letorozle treatment, 10–14 days following the start of treatment, and 90 days following the start of treatment. Samples were annotated as a "responder" (i.e., responds to letrozole treatment), a "non-responder" (i.e., no benefit from letrozole treatment), or "not assessable" (i.e., unknown). The Series Matrix Files were downloaded from Gene Expression Omnibus (GSE20181) and each gene of interest was extracted and processed into a text file. We used the following Affymetrix ID numbers 221359_at, 210683_at, 210237_at, 221373_x_at, and 211421_s_at, to represent *GDNF*, *NRTN*, *ARTN*, *PSPN*, and *RET* respectively. We found no evidence of differences in RET or RET ligand expression across the three time points, and we therefore used the average expression of each RET ligand in each sample when comparing between responsive and non-responsive patients in order to decrease assay noise.

Outlier scores were designed to score the degree to which each sample fell within the tail of the distribution representing high expression levels of each RET ligand (as shown in Fig 4F). Because endocrine resistance could, in principal, be caused either by high expression of any individual RET ligand on its own, or by moderately high expression of multiple RET ligands in combination, we devised a data transformation and sum approach to score the degree to which all four of the RET ligands were highly expressed in each sample. In our data transformation, expression levels were centered by the median value and scaled based on the lower tail of the expression distribution (between quartile 0 and 50). This approach is similar in concept to a Z-score transform, but uses the lower tail to estimate the variance in order to avoid having high expression levels, which we hypothesize here may contribute to endocrine resistance, from contributing to the denominator used to standardize the distribution of each RET ligand. After transforming scores from all four RET ligands separately, we took the sum of the scores to represent our final 'outlier score'. Because our hypothesis specifically predicted an increase in the RET ligand score to correlate with letrozole resistance, and because the number of patients was small, we designed the analysis to use a one-tailed Wilcoxon rank sum test. However, in practice, using a two-tailed Wilcoxon rank sum test did not change the results of our analysis. Data was processed and visualization was completed using R.

RNA isolation and quantitative real-time PCR

RNA was purified using an RNeasy Kit (Qiagen; Cat# 74104) and 1μg of purified RNA was reverse-transcribed using a High Capacity RNA-to-cDNA kit (Applied Biosystems; Cat# 4387406) according to the manufacturers' protocols. Real-time quantitative PCR analysis was performed using the following primers: *ACTB* Forward (5'-CCAACCGCGAGAAGATGA-3') and Reverse (5'- CCAGAGGCGTACAGGGATAG-3'); *ESR1* Forward (5'- TTACTGAC-CAACCTGGCAGA-3') and Reverse (5'-ATCATGGAGGGTCAAATCCA-3'); *PGR* Forward (5'-GTCAGGCTGGCATGGTCCTT-3') and Reverse (5'-GCTGTGGGAGAGCAACAGCA-3'); *GREB1* Forward (5'- GTGGTAGCCGAGTGGACAAT-3') and Reverse (5'-ATTTGTTTCCAGCCCTCCTT-3') [49]; *GDNF* Forward (5'- TCTGGGCTATGAAACCAAGGA-3') and Reverse (5'- GTCTCAGCTGCATCGCAAGA-3')[50]; and Power SYBR Green PCR Master

Mix (Applied Bioystems; Cat#4367659). The samples were normalized to β-actin. At least three biological replicates were performed and data are presented as mean ± SEM. All statistical analyses for qPCR were performed using GraphPad Prism. Groups were compared using a two-tailed unpaired Student's t-test.

Generation of GDNF knockdown G11 cells

GDNF expression was stably knocked down in G11^{TamR} cells by transduction with lentivirus expressing either a shRNA scrambled control or *GDNF* shRNA. Mission shRNA lentivirus plasmids for control shRNA (Cat# SHC002) and *GDNF* shRNA (Cat# SHCLND-NM_000514) from Sigma-Aldrich were used. Specifically, 1.5 μg pLKO.1 shRNA plasmid (Addgene; Plasmid #1864), 0.5 μg psPAX2 packaging plasmid (Addgene; Plasmid #12260), and 0.25 μg pMD2.G envelope plasmid were used for packaging (Addgene; Plasmid #12259). The lentiviruses were generated and transduced according to the manufacturer's instructions (Sigma-Aldrich). Clones were selected in 2 μg/ml of puromycin.

Cell proliferation assay

Approximately 1x10^6 G11-scrambled (G11-SCR) and G11-GDNF-knockdown (G11-GDNF-KD) cells were plated in T25 TC-flask. The cells were grown in either 0, 5 μM tamoxifen in the presence or absence of 5 ng/mL GDNF for 7 days. The cell number was counted for quantification and was normalized to the untreated group. Three biological replicates were performed.

Statistical analysis

Statistical parameters include the exact number of biological replicates (n), standard error of the mean (mean ± SEM), and statistical significance are reported in the figure legends. Data are reported statistically significant when $p < 0.05$ by two-tailed Student's t-test. In figures, asterisks and pound signs denote statistical significance as calculated by Student's t-test. Specific p-values are indicated in the figure legends. Statistical analysis was performed using GraphPad PRISM 6.

Supporting information

S1 Table. PRO-seq data collection and sequencing depth. PRO-seq was conducted in the indicated cell clone and biological condition. Raw PRO-seq data were sequenced to a read depth >20 million uniquely mapped reads and aligned using established pipelines. (DOCX)

S1 Fig. dREG identifies highly enriched active enhancers and promoter makers in MCF-7 cells. (**a**) Heatmap depicting PRO-seq, Dnase-I-seq, H3K27ac, and H3K4me3 near 39,753 transcriptional regulatory elements (TREs) identified using dREG-HD from PRO-seq data (left) in TamS and TamR MCF-7 cells. (**b**) Transcription and dREG scores in the locus near the *CCND1* gene in B7^{TamS} and G11^{TamR} MCF-7 cells. (**c**) Luciferase activity in B7^{TamS} and G11^{TamR} MCF-7 cells in the presence of an enhancer located approximately 300kb downstream of *CCND1*. All data normalized to renilla control. Data are represented as mean ± SEM (n = 3). ** $p < 0.01$, **** $p < 0.0001$. (EPS)

S2 Fig. GDNF induces fulvestrant resistance in TamS cells. (**a**) Cell viability of B7^{TamS} cells in the presence or absence of 10 ng/ml GDNF and/or 100 mM fulvestrant for 4 days. Data are

represented as mean ± SEM (n = 3). ** p < 0.005, **** p < 0.0001.
(EPS)

S3 Fig. RET ligand expression is low compared to RET and GFRα1 receptors. (**a**) Density scatterplot showing the relationship between *GFRA1* and *ESR1* expression levels in 1,177 primary breast cancer samples in the cancer genome atlas (TCGA). Pearson's R = 0.52; p < 2.2e-16. (**b**) Violin plots depicting the absolute normalized expression level of receptor-tyrosine kinase receptors and ligands in 1,177 primary breast cancer samples (TCGA). For each color, the pair of genes represents receptor (left) and ligand (right). Gray represents the *RET* gene which encodes the RET tyrosine kinase receptor required for signal transduction of all four RET ligands.
(EPS)

Acknowledgments

Author Contributions

Conceptualization: Sachi Horibata, Brooke A. Marks, Scott A. Coonrod, Charles G. Danko.

Data curation: Chinatsu Mukai, Kelly Sams, Charles G. Danko.

Formal analysis: Charles G. Danko.

Funding acquisition: Charles G. Danko.

Investigation: Sachi Horibata, Edward J. Rice, Chinatsu Mukai, Hui Zheng, Lynne J. Anguish, Charles G. Danko.

Methodology: Sachi Horibata, Edward J. Rice, Hui Zheng, Lynne J. Anguish, Charles G. Danko.

Project administration: Scott A. Coonrod, Charles G. Danko.

Resources: Charles G. Danko.

Software: Charles G. Danko.

Supervision: Scott A. Coonrod, Charles G. Danko.

Visualization: Sachi Horibata, Charles G. Danko.

Writing – original draft: Sachi Horibata, Charles G. Danko.

Writing – review & editing: Sachi Horibata, Scott A. Coonrod, Charles G. Danko.

References

1. Shiau AK, Barstad D, Loria PM, Cheng L, Kushner PJ, Agard DA, et al. The structural basis of estrogen receptor/coactivator recognition and the antagonism of this interaction by tamoxifen. Cell. 1998; 95: 927–37. Available: http://www.ncbi.nlm.nih.gov/pubmed/9875847 PMID: 9875847

2. Wakeling AE. Similarities and distinctions in the mode of action of different classes of antioestrogens. Endocr Relat Cancer. 2000; 7: 17–28. Available: http://www.ncbi.nlm.nih.gov/pubmed/10808193 PMID: 10808193

3. Musgrove EA, Sutherland RL. Biological determinants of endocrine resistance in breast cancer. Nat Rev Cancer. Nature Publishing Group; 2009; 9: 631–643. https://doi.org/10.1038/nrc2713 PMID: 19701242

4. Ma CX, Sanchez CG, Ellis MJ. Predicting endocrine therapy responsiveness in breast cancer. Oncology (Williston Park). 2009; 23: 133–42. Available: http://www.ncbi.nlm.nih.gov/pubmed/19323294

5. Gattelli A, Nalvarte I, Boulay A, Roloff TC, Schreiber M, Carragher N, et al. Ret inhibition decreases growth and metastatic potential of estrogen receptor positive breast cancer cells. EMBO Mol Med. 2013; 5: 1335–50. https://doi.org/10.1002/emmm.201302625 PMID: 23868506

6. Morandi A, Martin L-A, Gao Q, Pancholi S, Mackay A, Robertson D, et al. GDNF-RET signaling in ER-positive breast cancers is a key determinant of response and resistance to aromatase inhibitors. Cancer Res. 2013; 73: 3783–95. https://doi.org/10.1158/0008-5472.CAN-12-4265 PMID: 23650283

7. Plaza-Menacho I, Morandi A, Robertson D, Pancholi S, Drury S, Dowsett M, et al. Targeting the receptor tyrosine kinase RET sensitizes breast cancer cells to tamoxifen treatment and reveals a role for RET in endocrine resistance. Oncogene. 2010; 29: 4648–57. https://doi.org/10.1038/onc.2010.209 PMID: 20531297

8. Andreucci E, Francica P, Fearns A, Martin L-A, Chiarugi P, Isacke CM, et al. Targeting the receptor tyrosine kinase RET in combination with aromatase inhibitors in ER positive breast cancer xenografts. Oncotarget. Impact Journals, LLC; 2016; 7: 80543–80553. https://doi.org/10.18632/oncotarget.11826 PMID: 27602955

9. Gonzalez-Malerva L, Park J, Zou L, Hu Y, Moradpour Z, Pearlberg J, et al. High-throughput ectopic expression screen for tamoxifen resistance identifies an atypical kinase that blocks autophagy. Proc Natl Acad Sci U S A. 2011; 108: 2058–63. https://doi.org/10.1073/pnas.1018157108 PMID: 21233418

10. Hah N, Danko CG, Core L, Waterfall JJ, Siepel A, Lis JT, et al. A rapid, extensive, and transient transcriptional response to estrogen signaling in breast cancer cells. Cell. 2011; 145: 622–34. https://doi.org/10.1016/j.cell.2011.03.042 PMID: 21549415

11. Danko CG, Hah N, Luo X, Martins AL AL, Core L, Lis JT, et al. Signaling Pathways Differentially Affect RNA Polymerase II Initiation, Pausing, and Elongation Rate in Cells. Mol Cell. Elsevier; 2013; 50: 212–222. https://doi.org/10.1016/j.molcel.2013.02.015 PMID: 23523369

12. Mahat DB, Salamanca HH, Duarte FM, Danko CG, Lis JT. Mammalian Heat Shock Response and Mechanisms Underlying Its Genome-wide Transcriptional Regulation. Mol Cell. 2016; 62: 63–78. https://doi.org/10.1016/j.molcel.2016.02.025 PMID: 27052732

13. Duarte FM, Fuda NJ, Mahat DB, Core LJ, Guertin MJ, Lis JT. Transcription factors GAF and HSF act at distinct regulatory steps to modulate stress-induced gene activation. Genes Dev. 2016; 30: 1731–1746. https://doi.org/10.1101/gad.284430.116 PMID: 27492368

14. Arner E, Daub CO, Vitting-Seerup K, Andersson R, Lilje B, Drablos F, et al. Transcribed enhancers lead waves of coordinated transcription in transitioning mammalian cells. Science (80-). 2015; 347: 1010–1014. https://doi.org/10.1126/science.1259418 PMID: 25678556

15. Kim T-K, Hemberg M, Gray JM, Costa AM, Bear DM, Wu J, et al. Widespread transcription at neuronal activity-regulated enhancers. Nature. Macmillan Publishers Limited. All rights reserved; 2010; 465: 182–7. https://doi.org/10.1038/nature09033 PMID: 20393465

16. Hah N, Murakami S, Nagari A, Danko C, Kraus WL. Enhancer Transcripts Mark Active Estrogen Receptor Binding Sites. Genome Res. 2013; https://doi.org/10.1101/gr.152306.112 PMID: 23636943

17. Core LJ, Martins AL, Danko CG, Waters CT, Siepel A, Lis JT. Analysis of transcription start sites from nascent RNA supports a unified architecture of mammalian promoters and enhancers. Nat Genet. 2014;In Press.

18. Danko CG, Hyland SL, Core LJ, Martins AL, Waters CT, Lee HW, et al. Identification of active transcriptional regulatory elements from GRO-seq data. Nat Methods. Nature Publishing Group, a division of Macmillan Publishers Limited. All Rights Reserved.; 2015;advance on. https://doi.org/10.1038/nmeth.3329 PMID: 25799441

19. Andersson R, Gebhard C, Miguel-Escalada I, Hoof I, Bornholdt J, Boyd M, et al. An atlas of active enhancers across human cell types and tissues. Nature. Nature Publishing Group, a division of Macmillan Publishers Limited. All Rights Reserved.; 2014; 507: 455–461. https://doi.org/10.1038/nature12787 PMID: 24670763

20. Scruggs BS, Gilchrist DA, Nechaev S, Muse GW, Burkholder A, Fargo DC, et al. Bidirectional Transcription Arises from Two Distinct Hubs of Transcription Factor Binding and Active Chromatin. Mol Cell. Elsevier; 2015; 58: 1101–1112. https://doi.org/10.1016/j.molcel.2015.04.006 PMID: 26028540

21. Coser KR, Wittner BS, Rosenthal NF, Collins SC, Melas A, Smith SL, et al. Antiestrogen-resistant subclones of MCF-7 human breast cancer cells are derived from a common monoclonal drug-resistant progenitor. Proc Natl Acad Sci U S A. 2009; 106: 14536–41. https://doi.org/10.1073/pnas.0907560106 PMID: 19706540

22. Kwak H, Fuda NJ, Core LJ, Lis JT. Precise maps of RNA polymerase reveal how promoters direct initiation and pausing. Science. 2013; 339: 950–3. https://doi.org/10.1126/science.1229386 PMID: 23430654

23. Mahat DB, Kwak H, Booth GT, Jonkers IH, Danko CG, Patel RK, et al. Base-pair-resolution genome-wide mapping of active RNA polymerases using precision nuclear run-on (PRO-seq). Nat Protoc. 2016; 11: 1455–1476. https://doi.org/10.1038/nprot.2016.086 PMID: 27442863

24. Love MI, Huber W, Anders S. Moderated estimation of fold change and dispersion for RNA-seq data with DESeq2. Genome Biol. BioMed Central Ltd; 2014; 15: 550. https://doi.org/10.1186/s13059-014-0550-8 PMID: 25516281

25. Zhong Z, Shan M, Wang J, Liu T, Xia B, Niu M, et al. HOXD13 methylation status is a prognostic indicator in breast cancer. Int J Clin Exp Pathol. e-Century Publishing Corporation; 2015; 8: 10716–24. Available: http://www.ncbi.nlm.nih.gov/pubmed/26617782 PMID: 26617782

26. Ghoussaini M, Edwards SL, Michailidou K, Nord S, Cowper-Sal Lari R, Desai K, et al. Evidence that breast cancer risk at the 2q35 locus is mediated through IGFBP5 regulation. Nat Commun. 2014; 4: 4999. https://doi.org/10.1038/ncomms5999 PMID: 25248036

27. Mohammed H, D'Santos C, Serandour AA, Ali HR, Brown GD, Atkins A, et al. Endogenous purification reveals GREB1 as a key estrogen receptor regulatory factor. Cell Rep. 2013; 3: 342–9. https://doi.org/10.1016/j.celrep.2013.01.010 PMID: 23403292

28. Esseghir S, Todd SK, Hunt T, Poulsom R, Plaza-Menacho I, Reis-Filho JS, et al. A Role for Glial Cell Derived Neurotrophic Factor Induced Expression by Inflammatory Cytokines and RET/GFR 1 Receptor Up-regulation in Breast Cancer. Cancer Res. 2007; 67: 11732–11741. https://doi.org/10.1158/0008-5472.CAN-07-2343 PMID: 18089803

29. Azofeifa JG, Dowell RD. A generative model for the behavior of RNA polymerase. Bioinformatics. Oxford University Press; 2016; btw599. https://doi.org/10.1093/bioinformatics/btw599 PMID: 27663494

30. Chu T, Rice EJ, Booth GT, Salamanca HH, Wang Z, Core LJ, et al. Chromatin run-on reveals nascent RNAs that differentiate normal and malignant brain tissue. doi.org. Cold Spring Harbor Laboratory; 2017; 185991. https://doi.org/10.1101/185991

31. Wang Z, Martins AL, Danko CG. RTFBSDB: an integrated framework for transcription factor binding site analysis. Bioinformatics. Oxford University Press; 2016; btw338. https://doi.org/10.1093/bioinformatics/btw338 PMID: 27288497

32. Mohammed H, Russell IA, Stark R, Rueda OM, Hickey TE, Tarulli GA, et al. Progesterone receptor modulates ERα action in breast cancer. Nature. 2015; 523: 313–7. https://doi.org/10.1038/nature14583 PMID: 26153859

33. Welboren W-J, van Driel MA, Janssen-Megens EM, van Heeringen SJ, Sweep FC, Span PN, et al. ChIP-Seq of ERalpha and RNA polymerase II defines genes differentially responding to ligands. EMBO J. European Molecular Biology Organization; 2009; 28: 1418–28. https://doi.org/10.1038/emboj.2009.88 PMID: 19339991

34. Benz CC, Scott GK, Sarup JC, Johnson RM, Tripathy D, Coronado E, et al. Estrogen-dependent, tamoxifen-resistant tumorigenic growth of MCF-7 cells transfected with HER2/neu. Breast Cancer Res Treat. 1992; 24: 85–95. Available: http://www.ncbi.nlm.nih.gov/pubmed/8095168 PMID: 8095168

35. Sariola H, Saarma M. Novel functions and signalling pathways for GDNF. J Cell Sci. 2003;116.

36. Miller WR, Larionov A, Anderson TJ, Evans DB, Dixon JM. Sequential changes in gene expression profiles in breast cancers during treatment with the aromatase inhibitor, letrozole. Pharmacogenomics J. 2012; 12: 10–21. https://doi.org/10.1038/tpj.2010.67 PMID: 20697427

37. Kang J, Qian PX, Pandey V, Perry JK, Miller LD, Liu ET, et al. Artemin is estrogen regulated and mediates antiestrogen resistance in mammary carcinoma. Oncogene. Nature Publishing Group; 2010; 29: 3228–3240. https://doi.org/10.1038/onc.2010.71 PMID: 20305694

38. Stine ZE, McGaughey DM, Bessling SL, Li S, McCallion AS. Steroid hormone modulation of RET through two estrogen responsive enhancers in breast cancer. Hum Mol Genet. Oxford University Press; 2011; 20: 3746–56. https://doi.org/10.1093/hmg/ddr291 PMID: 21737465

39. The Cancer Genome Atlas Network. Comprehensive molecular portraits of human breast tumours. Nature. Nature Publishing Group, a division of Macmillan Publishers Limited. All Rights Reserved.; 2012; 490: 61–70. https://doi.org/10.1038/nature11412 PMID: 23000897

40. Ciriello G, Gatza ML, Beck AH, Wilkerson MD, Rhie SK, Pastore A, et al. Comprehensive Molecular Portraits of Invasive Lobular Breast Cancer. Cell. 2015; 163: 506–519. https://doi.org/10.1016/j.cell.2015.09.033 PMID: 26451490

41. Zhou Y, Eppenberger-Castori S, Marx C, Yau C, Scott GK, Eppenberger U, et al. Activation of nuclear factor-κB (NFκB) identifies a high-risk subset of hormone-dependent breast cancers. Int J Biochem Cell Biol. 2005; 37: 1130–1144. https://doi.org/10.1016/j.biocel.2004.09.006 PMID: 15743683

42. Franco HL, Nagari A, Kraus WL. TNFα Signaling Exposes Latent Estrogen Receptor Binding Sites to Alter the Breast Cancer Cell Transcriptome. Mol Cell. 2015; 58: 21–34. https://doi.org/10.1016/j.molcel.2015.02.001 PMID: 25752574

43. Core LJ, Waterfall JJ, Lis JT. Nascent RNA sequencing reveals widespread pausing and divergent initiation at human promoters. Science (80-). Department of Molecular Biology and Genetics, Cornell University, Ithaca, NY 14853, USA.; 2008; 322: 1845–1848. https://doi.org/10.1126/science.1162228 PMID: 19056941

44. Martin M. Cutadapt removes adapter sequences from high-throughput sequencing reads [Internet]. EMBnet journal. 2011. pp. 10–12. Available: http://journal.embnet.org/index.php/embnetjournal/article/view/200/479

45. Li H, Durbin R. Fast and accurate short read alignment with Burrows-Wheeler transform. Bioinformatics. 2009; 25: 1754–60. https://doi.org/10.1093/bioinformatics/btp324 PMID: 19451168

46. Quinlan AR, Hall IM. BEDTools: a flexible suite of utilities for comparing genomic features. Bioinformatics. 2010; 26: 841–2. https://doi.org/10.1093/bioinformatics/btq033 PMID: 20110278

47. Kuhn RM, Haussler D, Kent WJ. The UCSC genome browser and associated tools. Brief Bioinform. 2013; 14: 144–161. https://doi.org/10.1093/bib/bbs038 PMID: 22908213

48. Team RDC. R: A language and environment for statistical computing. In R Foundation for Statistical Computing [Internet]. Vienna, Austria: R Foundation for Statistical Computing; 2010. Available: http://www.r-project.org

49. Prenzel T, Begus-Nahrmann Y, Kramer F, Hennion M, Hsu C, Gorsler T, et al. Estrogen-Dependent Gene Transcription in Human Breast Cancer Cells Relies upon Proteasome-Dependent Monoubiquitination of Histone H2B. Cancer Res. 2011; 71: 5739–5753. https://doi.org/10.1158/0008-5472.CAN-11-1896 PMID: 21862633

50. Boulay A, Breuleux M, Stephan C, Fux C, Brisken C, Fiche M, et al. The Ret Receptor Tyrosine Kinase Pathway Functionally Interacts with the ER Pathway in Breast Cancer. Cancer Res. 2008; 68: 3743–3751. https://doi.org/10.1158/0008-5472.CAN-07-5100 PMID: 18483257